Intermetallics 30 (2012) 51–56

Contents lists available at SciVerse ScienceDirect

Intermetallics

journal homepage: www.elsevier.com/locate/intermet

Crystallization and martensitic transformation behavior of Ti–Ni–Sn alloy ribbons

Jae-hyun Kim [a], Hui-jin Choi [a], Min-soo Kim [a], Shuichi Miyazaki [a,b], Yeon-wook Kim [c], Byong Sun Chun [d], Tae-hyun Nam [a,*]

[a] School of Materials Science and Engineering & ERI, Gyeongsang National University, 900 Gazwadong, Jinju, Gyeongnam 660-701, Republic of Korea
[b] Institute of Materials Science, University of Tsukuba, Tsukuba, Ibaraki 305-8573, Japan
[c] Department of Advanced Materials Engineering, Keimyung University, 1000 Shindang-dong, Dalseo-gu, Daegu 704-701, Republic of Korea
[d] ReSEAT Program, KISTI, Daejeon, 305-806, South Korea

ARTICLE INFO

Article history:
Available online 8 May 2012

Keywords:
A. Nanostructured intermetallics
B. Martensitic transformation
C. Rapid solidification processing
F. Calorimetry
F. Diffraction

ABSTRACT

Crystallization behavior of rapidly solidified Ti–Ni–Sn alloys amorphous ribbons and martensitic transformation behavior after crystallization were examined by means of differential scanning calorimetry (DSC), X-ray diffraction (XRD) and transmission electron microscopy (TEM). Glass forming ability of Ti–Ni–Sn alloys increased with increasing Sn content and activation energy for crystallization increased from 151.2 ± 7.0 kJ/mol to 165.1 ± 9.0 kJ/mol with increasing Sn content from 5 at% to 7 at%, above which it almost kept constant. Crystallization occurs in the sequence of amorphous → $(Ti,Sn)_2Ni$ and B2 → B2 and Ti_3Sn when Sn content is ≤5 at%, amorphous → $(Ti,Sn)_2Ni$ → B2 → B2 and Ti_3Sn when Sn content is in the range of 5 at% and 10 at%, amorphous → $(Ti,Sn)_2Ni$ → Ti_3Sn → B2 and Ti_3Sn when Sn content is ≥10 at%. The crystallized Ti–Ni–Sn alloys showed the B2-R-B19′ martensitic transformation behavior. Rapid solidification was effective to separate the B2-R transformation from the R-B19′ transformation in Ti–Ni–Sn alloys.

1. Introduction

The B2 (cubic) – R (trigonal) phase transformation has attracted attentions of many researchers because of small transformation hysteresis. Several methods for inducing the R phase in Ti–Ni alloys have been developed such as annealing at moderate temperature after cold working [1,2], aging of Ni-rich alloys [3,4], rapid solidification [5,6] and the third elements addition [7–11] Iron [7], molybdenum [8], chromium [9], aluminum [10] and cobalt [11] are known to be effective for inducing the R phase transformation in Ti–Ni alloys.

Recently, Sn is known to be also effective for inducing the R phase in Ti–Ni alloys [12]. Ti–Ni–Sn alloys consist of the B2 (Ti–Ni phase containing Sn less than 1 at%) and the Ti_3Sn phases [12,13] and undergo the two-stage B2-R-B19′ martensitic transformation [12]. The Ti–Ni–Sn alloys with Sn content less than 8 at% (hypereutectic alloys) are deformed in ductile manner, while those with Sn content more than 10 at% are brittle. Unfortunately, the B2-R transformation and the R-B19′ transformation are not separated completely in the hypereutectic Ti–Ni–Sn alloys [12]. Rapid solidification is known to increase a temperature gap between the B2-R transformation start temperature (T_R) and the R-B19′ transformation start temperature (M_S) in Ti–Ni alloys, which was ascribed to very fine particles such as Ti_2Ni with an average size less than 50 nm [14]. Therefore, rapid solidification is expected to separate the B2-R from the R-B19′ completely in Ti–Ni–Sn alloys. In the present study, Ti–Ni–Sn alloy ribbons were prepared by melt spinning and then microstructures and martensitic transformation behavior were investigated.

2. Experimental procedure

Ti-40Ni-5Sn, Ti-36Ni-7Sn, Ti-34Ni-8Sn, Ti-32Ni-9Sn and Ti-30Ni-10Sn (at%) pre-alloy ingots were prepared by arc melting. The ingots were cut into billets and they were placed into quartz crucibles of internal diameter 10 mm and the chamber of the melt spinning system had been evacuated to less than 1×10^{-3} Pa before re-melting. When the melt temperature reached the expected temperature, it was ejected through the alumina nozzle with a circular shaped orifice on the outer surface of the rotating quenching wheel (30 cm in diameter) made of copper. Melt spinning temperature was 1773 K and the diameter of the orifice was 0.5 mm. The ejection pressure was 40 kPa and distance from the tip of the nozzle to the wheel surface was 300 μm. The linear speed of quenching wheel was kept at 40.0 m/s.

As-spun ribbons were annealed for crystallization by heating up to specific temperatures with heating rate of 0.33 K/s in differential

* Corresponding author. Tel.: +82 55 772 1665; fax: +82 55 772 5286.
E-mail address: tahynam@gnu.ac.kr (T.-h. Nam).

0966-9795/$ – see front matter © 2012 Elsevier Ltd. All rights reserved.
doi:10.1016/j.intermet.2012.03.040

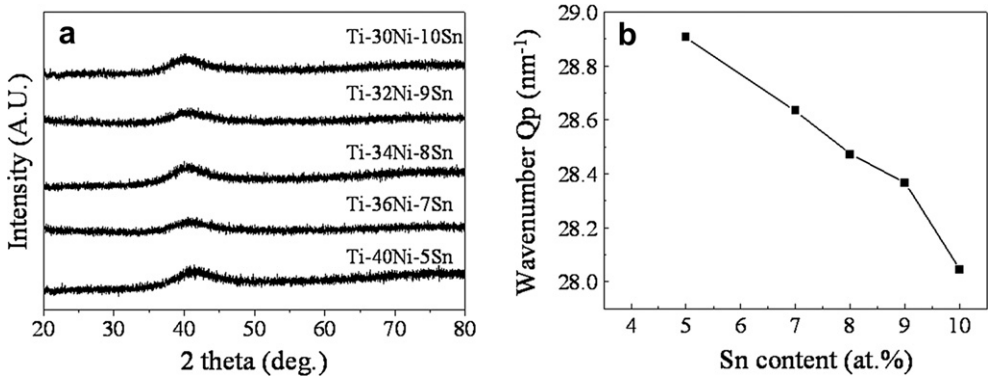

Fig. 1. (a) XRD patterns of as-spun Ti–Ni–Sn alloy ribbons. (b) Relationship between wave number and Sn content.

scanning calorimetry (DSC) equipment. Transmission electron microscope (TEM) observations were made using JEOL 2010 operated at an accelerating voltage of 200 kV. Thin foils for TEM observations were prepared by twin jet electropolishing in an electrolyte of 95% acetic acid and 5% perchloric acid by volume. The crystal structures of the ribbons were investigated by X-ray diffraction (XRD) using CuK_α radiation with successively changing experimental temperatures. For the study of martensitic transformation behaviors of the ribbons, DSC measurements were at heating and cooling rate of 0.17 K/s using TA Instrument DSC-2010.

3. Results and discussion

3.1. Crystallization behavior of Ti–Ni–Sn alloys

Fig. 1(a) shows the XRD patterns obtained from as-spun Ti–Ni–Sn alloy ribbons. A broad peak is found at $2\theta = 42^\circ$ in all patterns, which means that all the ribbons are amorphous. Since wave number (Q_p) is defined as $4\pi\sin\theta/\lambda$, where θ and λ are diffraction angle and wavelength of X-ray, respectively, and inversely proportional to the mean nearest-neighbor distance of local ordering clusters of amorphous alloys [15], the glass forming ability becomes larger as Q_p becomes smaller. From Fig. 1(a), Q_p is calculated and then plotted against Sn content in Fig. 1(b). It is found that Q_p decreases from 28.91 nm^{-1} to 28.07 nm^{-1} with increasing Sn content from 5 at% to 10 at%. Therefore, it is concluded that the glass forming ability of Ti–Ni–Sn alloy increases with increasing Sn content.

In order to determine activation energy for crystallization, DSC measurements were made at various heating rates of 0.08 K–0.42 K/s Fig. 2(a) shows typical DSC curves of Ti–Ni–Sn alloy ribbons obtained at a heating rate of 0.33 K/s. Several exothermic peaks are observed in all samples, which mean that crystallization occurs in multi steps. The Kissinger's plot for determining the activation energy for crystallization (E_a) was made on Ti–Ni–Sn alloy ribbons and then E_a obtained was plotted against Sn content in Fig. 2(b). E_a is found to increase from 151.2 ± 7.0 kJ/mol to 165.1 ± 9.0 kJ/mol with increasing Sn content from 5 at% to 7 at%, above which it almost keeps constant. E_a of Ti–Ni–Sn alloys is very small comparing with those of Ti–Ni and Ti–Ni–Cu alloys (usually 350–470 kJ/mol) [16–19]. The discrepancy is ascribed to the fact that activation energy of Ti–Ni and Ti–Ni–Cu alloys corresponds to crystallization of the B2 phase, while that of Ti–Ni–Sn alloys is due to crystallization of $(Ti,Sn)_2Ni$ as will be mentioned later.

In order to clarify crystallization behavior of amorphous Ti–Ni–Sn alloy ribbons, XRD patterns were obtained from samples which heating was stopped at various temperatures designated by

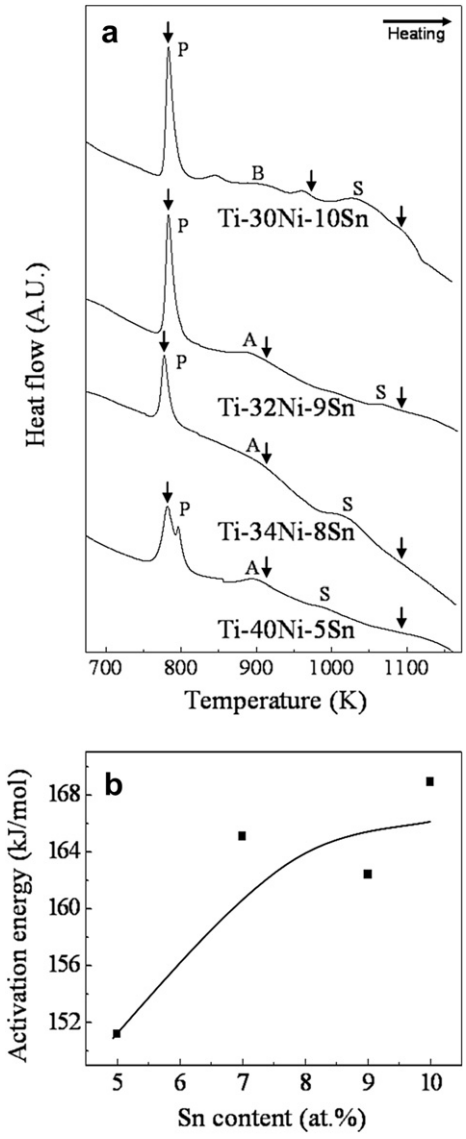

Fig. 2. (a) Typical DSC curves of Ti–Ni–Sn alloy ribbons obtained at the heating rate of 0.33 K/s. (b) Relationship between activation energy for crystallization and Sn content.